Observation and analysis of single and multiple high-order Laguerre-Gaussian beams generated from a hemi-cylindrical cavity with general astigmatism

T. H. Lu* and Y.C. Wu

Department of physics, National Taiwan Normal University, 88 Tingchou Road, Sec. 4, Taipei 11677, Taiwan
thlu@ntnu.edu.tw

Abstract: We experimentally verified that anisotropic Hermite-Gaussian modes can be generated from a hemi-cylindrical laser cavity and can be transformed into high-order Laguerre-Gaussian modes using an extra-cavity cylindrical lens. We further combined the Huygens integral and the ABCD law to clearly demonstrate the transformation along the propagation direction. By controlling the pump offset and the pump size in hemi-cylindrical cavities, we experimentally observed the unique laser patterns that displayed the optical waves related to the coherent superposition of Laguerre-Gaussian modes.

OCIS codes: (140.3480) Lasers, diode-pumped; (140.4780) Optical resonators; (070.2580) Paraxial wave optics; (030.4070) Modes.

References and links

1. J. Fu, Z. Si, S. Tang, and J. Deng, "Classical simulation of quantum entanglement using optical transverse modes in multimode waveguides," Phys. Rev. A **70**(4), 042313 (2004).
2. N. K. Langford, R. B. Dalton, M. D. Harvey, J. L. O'Brien, G. J. Pryde, A. Gilchrist, S. D. Bartlett, and A. G. White, "Measuring entangled qutrits and their use for quantum bit commitment," Phys. Rev. Lett. **93**(5), 053601 (2004).
3. K. Wagner, J. Janousek, V. Delaubert, H. Zou, C. Harb, N. Treps, J. F. Morizur, P. K. Lam, and H.-A. Bachor, "Entangling the spatial properties of laser beams," Science **321**(5888), 541–543 (2008).
4. D. Kawase, Y. Miyamoto, M. Takeda, K. Sasaki, and S. Takeuchi, "Effect of high-dimensional entanglement of Laguerre-Gaussian modes in parametric downconversion," J. Opt. Soc. Am. B **26**(4), 797–804 (2009).
5. T. Kuga, Y. Torii, N. Shiokawa, T. Hirano, Y. Shimizu, and H. Sasada, "Novel optical trap of atoms with a doughnut beam," Phys. Rev. Lett. **78**(25), 4713–4716 (1997).
6. L. Allen, M. W. Beijersbergen, R. J. C. Spreeuw, and J. P. Woerdman, "Orbital angular momentum of light and the transformation of Laguerre-Gaussian laser modes," Phys. Rev. A **45**(11), 8185–8189 (1992).
7. G. Gibson, J. Courtial, M. J. Padgett, M. Vasnetsov, V. Pas'ko, S. Barnett, and S. Franke-Arnold, "Free-space information transfer using light beams carrying orbital angular momentum," Opt. Express **12**(22), 5448–5456 (2004).
8. M. Lassen, V. Delaubert, J. Janousek, K. Wagner, H.-A. Bachor, P. K. Lam, N. Treps, P. Buchhave, C. Fabre, and C. C. Harb, "Tools for multimode quantum information: Mmodulation, detection, and spatial quantum correlations," Phys. Rev. Lett. **98**(8), 083602 (2007).
9. A. E. Kaplan, I. Marzoli, W. E. Lamb, Jr., and W. P. Schleich, "Multimode interference: Highly regular pattern formation in quantum wave-packet evolution," Phys. Rev. A **61**(3), 032101 (2000).
10. G. Nienhuis and L. Allen, "Paraxial wave optics and harmonic oscillators," Phys. Rev. A **48**(1), 656–665 (1993).
11. B. L. Johnson and G. Kirczenow, "Enhanced dynamical symmetries and quantum degeneracies in mesoscopic quantum dots: Role of the symmetries of closed classical orbits," Europhys. Lett. **51**(4), 367–373 (2000).
12. M. S. Soskin and M. V. Vasnetsov, "Singular optics," Prog. Opt. **42**, 219–276 (2001).
13. K. F. Huang, Y. F. Chen, H. C. Lai, and Y. P. Lan, "Observation of the wave function of a quantum billiard from the transverse patterns of vertical cavity surface emitting lasers," Phys. Rev. Lett. **89**(22), 224102 (2002).
14. T. Gensty, K. Becker, I. Fischer, W. Elsässer, C. Degen, P. Debernardi, and G. P. Bava, "Wave chaos in real-world vertical-cavity surface-emitting lasers," Phys. Rev. Lett. **94**(23), 233901 (2005).
15. E. J. Galvez, P. R. Crawford, H. I. Sztul, M. J. Pysher, P. J. Haglin, and R. E. Williams, "Geometric phase associated with mode transformations of optical beams bearing orbital angular momentum," Phys. Rev. Lett. **90**(20), 203901 (2003).
16. I. Vorobeichik, E. Narevicius, G. Rosenblum, M. Orenstein, and N. Moiseyev, "Electromagnetic realization of orders-of-magnitude tunneling enhancement in a double well system," Phys. Rev. Lett. **90**(17), 176806 (2003).

#197102 - $15.00 USD Received 13 Sep 2013; revised 25 Oct 2013; accepted 5 Nov 2013; published 12 Nov 2013

17. M. Brambilla, F. Battipede, L. A. Lugiato, V. Penna, F. Prati, C. Tamm, and C. O. Weiss, "Transverse laser patterns. I. Phase singularity crystals," Phys. Rev. A **43**(9), 5090–5113 (1991).
18. D. Dangoisse, D. Hennequin, C. Lepers, E. Louvergneaux, and P. Glorieux, "Two-dimensional optical lattices in a CO_2 laser," Phys. Rev. A **46**(9), 5955–5958 (1992).
19. S. Danakas and P. K. Aravind, "Analogies between two optical systems (photon beam splitters and laser beams) and two quantum systems (the two-dimensional oscillator and the two-dimensional hydrogen atom)," Phys. Rev. A **45**(3), 1973–1977 (1992).
20. M. W. Beijersbergen, L. Allen, H. E. L. O. van der Veen, and J. P. Woerdman, "Astigmatic laser mode converters and transfer of orbital angular momentum," Opt. Commun. **96**(1-3), 123–132 (1993).
21. J. Arlt, K. Dholakia, L. Allen, and M. J. Padgett, "The production of multiringed Laguerre–Gaussian modes by computer-generated holograms," J. Mod. Opt. **45**(6), 1231–1237 (1998).
22. N. Matsumoto, T. Ando, T. Inoue, Y. Ohtake, N. Fukuchi, and T. Hara, "Generation of high-quality higher-order Laguerre-Gaussian beams using liquid-crystal-on-silicon spatial light modulators," J. Opt. Soc. Am. A **25**(7), 1642–1651 (2008).
23. A. A. Ishaaya, N. Davidson, and A. A. Friesem, "Very high-order pure Laguerre-Gaussian mode selection in a passive Q-switched Nd:YAG laser," Opt. Express **13**(13), 4952–4962 (2005).
24. Y. Chen, Y. Lan, and S. Wang, "Generation of Laguerre-Gaussian modes in fiber-coupled laser diode end pumped lasers," Appl. Phys. B **72**(2), 167–170 (2001).
25. M. P. Thirugnanasambandam, Yu. Senatsky, and K. Ueda, "Generation of very-high order Laguerre-Gaussian modes in Yb:YAG ceramic laser," Laser Phys. Lett. **7**(9), 637–643 (2010).
26. J. A. Arnaud and H. Kogelnik, "Gaussian light beams with general astigmatism," Appl. Opt. **8**(8), 1687–1693 (1969).
27. J. Visser and G. Nienhuis, "Orbital angular momentum of general astigmatic modes," Phys. Rev. A **70**(1), 013809 (2004).
28. S. J. M. Harbraken and G. Nienhuis, "Modes of a twisted optical cavity," Phys. Rev. A **75**(3), 033819 (2007).
29. G. Nienhuis and J. Visser, "Angular momentum and vortices in paraxial beams," J. Opt. A, Pure Appl. Opt. **6**(5), S248–S250 (2004).
30. A. E. Siegman, *Lasers* (University Science, 1986).
31. J. J. Sakurai, *Modern Quantum Mechanics* (Addison-Wesley, 1994).
32. E. J. Galvez, P. R. Crawford, H. I. Sztul, M. J. Pysher, P. J. Haglin, and R. E. Williams, "Geometric phase associated with mode transformations of optical beams bearing orbital angular momentum," Phys. Rev. Lett. **90**(20), 203901 (2003).
33. Y. C. Lin, T. H. Lu, K. F. Huang, and Y. F. Chen, "Generation of optical vortex array with transformation of standing-wave Laguerre-Gaussian mode," Opt. Express **19**(11), 10293–10303 (2011).
34. T. H. Lu, Y. C. Lin, Y. F. Chen, and K. F. Huang, "Generation of multi-axis Laguerre-Gaussian beams from geometric modes of a hemiconfocal cavity," Appl. Phys. B **103**(4), 991–999 (2011).
35. J. L. Blows and G. W. Forbes, "Mode characteristics of twisted resonators composed of two cylindrical mirrors," Opt. Express **2**(5), 184–190 (1998).
36. H. Weber, "Rays and fields in general astigmatic resonators," J. Mod. Opt. **59**(8), 740–770 (2012).
37. Y. F. Chen, T. H. Lu, K. W. Su, and K. F. Huang, "Devil's staircase in three-dimensional coherent waves localized on Lissajous parametric surfaces," Phys. Rev. Lett. **96**(21), 213902 (2006).
38. T. H. Lu, Y. C. Lin, Y. F. Chen, and K. F. Huang, "Three-dimensional coherent optical waves localized on trochoidal parametric surfaces," Phys. Rev. Lett. **101**(23), 233901 (2008).
39. T. H. Lu, Y. C. Lin, Y. F. Chen, and K. F. Huang, "Generation of multi-axis Laguerre–Gaussian beams from geometric modes of a hemiconfocal cavity," Appl. Phys. B **103**(4), 991–999 (2011).

1. Introduction

Optical spatial mode generation has recently attracted considerable interest in branches of modern physics such as quantum entanglement [1–4], optical trapping [5], transfer of optical angular momentum [6], and information processing [7,8]. The propagation of a coherent optical wave inside a laser cavity is similar to the propagation of a quantum wave inside a mesoscopic structure [9]. The important analogy implies that the Hermite-Gaussian (HG) modes and Laguerre-Gaussian (LG) modes are identical to the rectangular and circular eigenstates of the two-dimensional harmonic oscillator [10–12]. Constructing optical waves is crucial and beneficial to realize numerous quantum signatures in an optical context, such as quantum chaos phenomena [13,14], geometric phases [15], and quantum tunneling [16]. Recently, various laser systems have been widely used to study optical pattern formation including LG modes, HG modes, and the transformation between the two families [17–19]. The systematic generation of optical transverse modes is one of the major concerns in developing the connection between optical waves and quantum waves.

A LG beam characterized by orbital angular momentum is one of the most essential features of optical waves. The approaches for generating LG beams can be broadly divided into two categories: intra- and extra-cavity approaches. Shaping the beam profile out of the

#197102 - $15.00 USD Received 13 Sep 2013; revised 25 Oct 2013; accepted 5 Nov 2013; published 12 Nov 2013

cavity to generate LG beams involves using an astigmatic mode converter [20], computer hologram [21], and spatial light modulator [22]. Conversely, a spatial transverse mode can be selected by inserting an intra-cavity element or manipulating the pump profile to achieve low energy losses for a specific LG mode [23,24]. The intra-cavity method is more efficient than the extra-cavity method for generating high-order LG beams because the extra-cavity scheme may be limited by optical elements [25]. Although the transformation from HG modes to LG modes has been successfully reconstructed for low-order and single modes, no study has focused on the transformation of HG modes into LG modes for high-order and multiple modes using a compact experimental setup.

In this study, we first experimentally verified that anisotropic HG modes generated from a hemi-cylindrical laser cavity can be transformed into high-order LG beams accompanied by the astigmatic compensation of an extra-cavity cylindrical lens. By combining the ABCD law and Huygens integral, the optical waves were clearly demonstrated under propagation. Furthermore, we experimentally employed off-axis and defocusing pumps to manipulate the output LG modes from low to high order and from single to multiple. The superposition of the LG modes revealed intriguing optical transverse patterns. Because the laser cavity is a well-defined analog system used for studying quantum waves, the present findings are useful for understanding the fundamental behavior of wave functions under the condition of a deformed harmonic oscillator with perturbation.

2. Experimental apparatus and propagation of astigmatic Hermite-Gaussian modes

The laser system was a diode-pumped Nd:YVO_4 laser. The cavity composed of a cylindrical mirror and a gain medium with coating is referred to as a simple astigmatic resonator [26]. Figure 1 shows a schematic diagram of the laser cavity arrangement. A cylindrical concave mirror with a radius of curvature of $R = 12\,\mathrm{mm}$ was used as a front mirror, and its reflectivity was 99.8% at 1064 nm. The cavity length was set as $L < R$ to provide a stable cavity. The

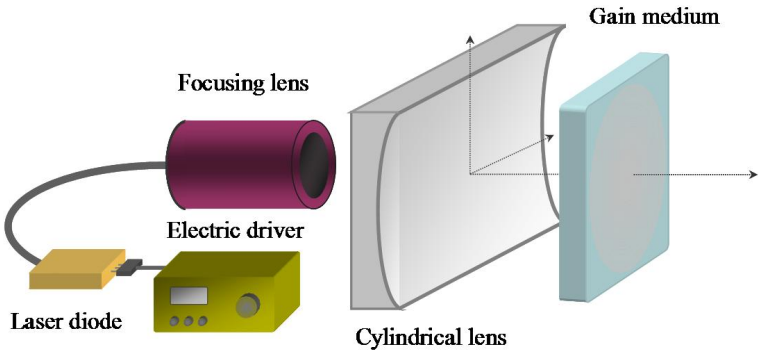

Fig. 1. Experimental setup for the generation of astigmatic HG beams using a diode-pumped microchip laser with an off-axis pumping scheme in a hemi-cylindrical cavity.

laser gain medium was an a-cut 2.0-at. % Nd:YVO_4 crystal with a length of $2\,\mathrm{mm}$. One side of the Nd:YVO_4 crystal was coated for antireflection at 1064 nm; the other side was coated as an output coupler with a reflectivity of 99%. The pump source was an 809 nm fiber-coupled laser diode with a core diameter of $100\,\mu\mathrm{m}$, a numerical aperture of 0.16, and maximal power of 3 W. A focusing lens with a $20\,\mathrm{mm}$ focal length and 90% coupling efficiency was used to guide the pump beam into the laser crystal. It was mounted on a two-dimensional mechanical stage to adjust the pump offset to excite high-order spatial modes. The level of astigmatism that developed from the anisotropic transverse boundary was considerable in the hemi-cylindrical cavity. In addition, the pumping profile guided onto the gain medium was altered to be anisotropic by passing through the cylindrical front mirror. The transverse

#197102 - $15.00 USD Received 13 Sep 2013; revised 25 Oct 2013; accepted 5 Nov 2013; published 12 Nov 2013

profile of a fundamental mode differs from the mode generated from a traditional spherical cavity and is propagation variant along the z- axis. Figures 2(a)–2(e) show the experimental results for the transverse profiles of the fundamental anisotropic Gaussian beam along the propagation direction. The cavity length was fixed at $L = 5$ mm . The intensity of the near-field image was clearly more focused in the y direction than in the x direction because of the difference between the radii of curvature in the x and y directions of the cylindrical mirror. The line-shape near-field image gradually became isotropic at the position $z = 5.0\,L$, and the image subsequently became a vertical lineshape at the far field. Because the boundary of the laser cavity was anisotropic, the pump offset along the y-axis sufficiently contributed to the generation of transverse high-order modes. To achieve the high-order mode, the cavity length and the pump offset were fixed at $8\,\text{mm}$ and $100\,\mu\text{m}$, respectively. Figures 3(a)–3(e) show the experimental results for the anisotropic $HG_{0,6}$ mode along the propagation direction. The tomogram clearly displays the structural variation in the shape of the astigmatic high-order HG mode, which differed from that of the traditional HG mode.

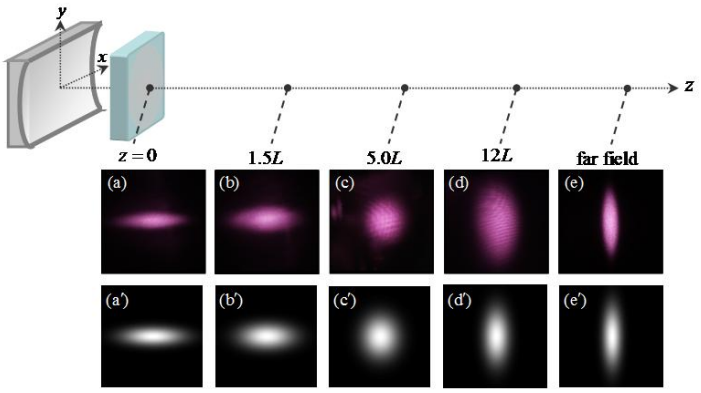

Fig. 2. (a)–(e): Experimental tomographic transverse patterns of the astigmatic $HG_{0,0}$ mode from the near field to the far field. (a')–(e'): Numerically reconstructed patterns for the experimental results.

3. Theoretical analyses for the propagation of astigmatic Hermite-Gaussian modes

The astigmatic Gaussian modes of paraxial wave equation and the relation between Gaussian modes of various orders are explicitly presented by an operator method [10,27–29]. The methods and results can be applied to the evolution of a particle in free space because of the analogy between the paraxial wave equation and the Schrödinger equation. In this section, we used the Huygens integral to convert the laser modes emitted from the hemi-cylindrical cavity through an ABCD optical system. The Huygens integral of an input beam of a high-order HG mode in one transverse dimension associated with an ABCD matrix of length *d* can be given by

$$u_n(x,z) = \sqrt{\frac{i}{B\lambda}}\, e^{-ikd} \times \int_{-\infty}^{\infty} u_n(x_0,z_0) \exp\left[-i\frac{\pi\left(Ax_0^2 - 2x_0 x + Dx^2\right)}{B\lambda}\right] dx_0 \qquad (1)$$

where *k* is the wave number and λ is the wavelength in free space. The input HG mode can be represented as [30]

$$u_n(x_0,z_0) = \sqrt{\frac{\sqrt{2}}{2^n n!\omega_0\sqrt{\pi}}}\, H_n\left(\frac{\sqrt{2}x_0}{\omega_0}\right) \exp\left[-i\frac{\pi x_0^2}{\lambda q_0}\right] \qquad (2)$$

#197102 - $15.00 USD Received 13 Sep 2013; revised 25 Oct 2013; accepted 5 Nov 2013; published 12 Nov 2013

where ω_0 is the beam waist, q_0 is the q parameter at the beam waist, and $H_n(.)$ is a Hermite polynomial of order n. After performing a complex algebraic calculation, the one-dimensional HG mode traveling through an arbitrary optical system of the ABCD matrix can be modified as

$$u_n(x,z)=\sqrt{\frac{\sqrt{2}}{2^n n!\omega_0\sqrt{\pi}}}\left(\frac{1}{A+B/q_0}\right)^{n+\frac{1}{2}}\left(\frac{\omega}{\omega_0}\right)^n H_n\left(\frac{\sqrt{2}x}{\omega}\right)\exp\left[-i\frac{\pi x^2}{\lambda q}\right] \qquad (3)$$

where $q=(Aq_0+B)/(Cq_0+D)$ and $\omega=\omega_0\left((A+B/q_0)^2+i\left[2B\lambda(A+B/q_0)/\pi\omega_0^2\right]\right)^{1/2}$. The phase term $\exp(-ikd)$ in Eq. (1) was neglected because it does not affect the intensity distribution. By considering the hemi-cylindrical cavity as an anisotropic two-dimensional system, the general field distribution of the two-dimensional HG mode expanded from Eq. (3) can be written as

$$\begin{aligned}u_{n,m}(x,y,z)&=u_n(x,z)\cdot u_m(y,z)\\&=\sqrt{\frac{1}{2^{n+m-1}\pi n!m!\omega_{0x}\omega_{0y}}}\left(\frac{1}{A_x+B_x/q_{0x}}\right)^{n+1/2}\left(\frac{1}{A_y+B_y/q_{0y}}\right)^{m+1/2}\left(\frac{\omega_x}{\omega_{0x}}\right)^n\left(\frac{\omega_y}{\omega_{0y}}\right)^m \qquad (4)\\&\times H_n\left(\frac{\sqrt{2}x}{\omega_x}\right)H_m\left(\frac{\sqrt{2}y}{\omega_y}\right)\exp\left[-i\frac{\pi x^2}{\lambda q_x}\right]\exp\left[-i\frac{\pi y^2}{\lambda q_y}\right]\end{aligned}$$

Therefore, we can conveniently apply Eq. (4) to describe the anisotropic HG modes passing through an arbitrary optical system with a simple 2×2 matrix. To interpret the experimental results in Figs. 2(a)–2(e) and Figs. 3(a)–3(e) by Eq. (4), the effective radius of curvature induced by the thermal lens effect should be determined first. A thermal lens effect caused by the thermal gradient in the gain medium provides confinement for the transverse mode in the x-axis direction. The effective radius of curvature induced by the thermal lens effect was verified to be $1000\,\text{mm}$, which corresponded to the experimental results shown in Figs. 2(a)–2(e). The curvature of the cylindrical lens was placed along the y-axis as $R_y=12\,\text{mm}$, and the cavity length was fixed at $L=5\,\text{mm}$. The propagation matrix for the lasing modes emitted from the hemi-cylindrical cavity can be represented as

$$M_x(z)=M_y(z)=\begin{pmatrix}1 & z\\ 0 & 1\end{pmatrix}. \qquad (5)$$

Substituting the parameters into Eq. (4), the numerical results for the lasing modes under propagation can be revealed. Figures 2(a')–2(e') show the numerical results for the transverse beam profiles from $z=0$ to the far field; these results are consistent with the experimental results. The difference between the two radii of curvature along the orthogonal axes indicates that the astigmatic fundamental mode was generated from the hemi-cylindrical cavity. The beam waist along the y-axis was approximately 4 times smaller than that along the x-axis. By contrast, the divergence angle in the y direction was approximately 4 times larger than that in the x direction. The radius of curvature resulting from the thermal lens effect along the x-axis was $5000\,\text{mm}$, which corresponds to the experimental result presented in Figs. 3(a)–3(e). Figures 3(a')–3(e') show the numerical results for the transverse beam profiles of the $HG_{0,6}$ mode from $z=0$ to the far field.

#197102 - $15.00 USD Received 13 Sep 2013; revised 25 Oct 2013; accepted 5 Nov 2013; published 12 Nov 2013

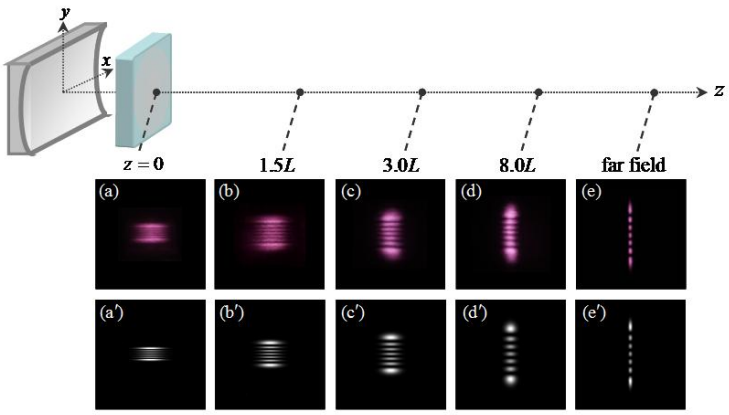

Fig. 3. (a)–(e): Experimental tomographic transverse patterns of the astigmatic $HG_{0,6}$ mode at $z = 0$, $1.5L$, $3.0L$, $8.0L$, and far field. (a')–(e'): Numerically reconstructed patterns for the experimental results.

The effective radius of curvature caused by the thermal lens effect depends on several parameters of the laser cavity, such as the pump offset, the degree of defocus, and cavity lengths. A large astigmatism was induced by the hemi-cylindrical cavity and caused the generation of anisotropic Hermite-Gaussian modes with various aspect ratios under propagation. In addition, the off-axis pump was useful in generating the various high-order astigmatic HG modes. The numerical results are in a good agreement with the experimental results.

4. Transformation from astigmatic Hermite-Gaussian modes to Laguerre-Gaussian modes

The transformation between isotropic HG modes and LG modes by use of mode converters is experimentally and theoretically analyzed [20]. The transformation from HG modes to LG modes must fulfill the mode-matching condition. To modify the differing divergence angle of the lasing modes emitted from the hemi-cylindrical cavity, an extra-cavity plano-convex cylindrical lens with a focal length of 2 cm was placed at a distance of 2 cm from the beam waist and rotated to an angle of $\theta = 40^{\circ}$ to transform the lasing modes. Figures 4(a)–4(e) show the experimental transverse profile of the astigmatic $HG_{0,0}$ mode from the near field to the far field after transformation. The cavity length was fixed at $L = 5$ mm. The added cylindrical lens modified the divergence angle and altered the phase of the astigmatic HG modes.

#197102 - $15.00 USD Received 13 Sep 2013; revised 25 Oct 2013; accepted 5 Nov 2013; published 12 Nov 2013

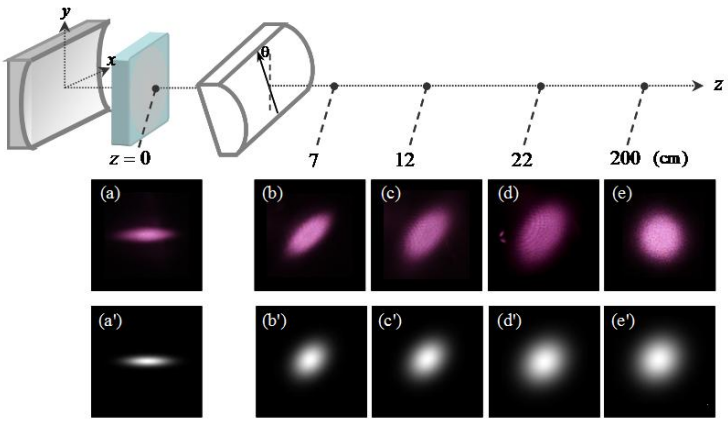

Fig. 4. (a)–(e): Experimental results of the transformation from astigmatic $HG_{0,0}$ mode to LG mode. (a')–(e'): Numerically reconstructed patterns for the experimental results.

The anisotropic $HG_{0,0}$ mode is transformed into $LG_{0,0}$ mode. To explain the transformation behavior of the mode with the result of Fresnel integral, we have to find the new basis which corresponds to the same axes (x_1 and y_1 axes) of the added cylindrical lens. Consequently, we expanded the rotated HG mode into a set of HG bases without rotation and determined the weighting coefficient to achieve the effect caused by an extra-cavity cylindrical lens with an angle θ. Using the generating function and an algebraic calculation, the rotated HG mode with the same axes of the extra-cavity cylindrical lens can be expressed in the elegant form:

$$u_{n,m}(x_1,y_1,z)=\sum_{s=0}^{N} d^{\frac{N}{2}}_{s-\frac{N}{2},n-\frac{N}{2}}(\theta)\,u_{s,N-s}(x,y,z) \tag{6}$$

where $x_1 = x\cos\theta + y\sin\theta$, $y_1 = x(-\sin\theta) + y\cos\theta$, $N = n+m$, and

$$d^{\frac{N}{2}}_{s-\frac{N}{2},n-\frac{N}{2}}(\theta)=\sqrt{s!}\sqrt{(N-s)!}\sqrt{n!}\sqrt{(N-n)!} \times \sum_{v=\max[0,s-n]}^{\min[N-n,s]} \frac{(-1)^v\left[\cos\left(\frac{\theta}{2}\right)\right]^{n+s-2v}\left[\sin\left(\frac{\theta}{2}\right)\right]^{m-s+2v}}{v!(N-n-v)!(s-v)!(n-s+v)!}. \tag{7}$$

The weighting coefficient, Eq. (7), of the HG basis without rotation is the same as Wigner *d*-coefficient [31]. It revealed the equivalence of the basis in Eq. (6) and a basis represented by SU(2) transform. By substituting Eq. (4) into (6), the field distribution of the astigmatic HG modes traveling through a cylindrical lens with an angle of rotation θ can be clearly demonstrated. Figures 4(a')–4(e') display the numerical results according to the experimental patterns in Figs. 4(a)–4(e). The corresponding parameters of the numerical results were $R_x = 1500$ mm, $R_y = 12$ mm, $L = 5$ mm, $\theta = 40^{\circ}$, and the focal length of the extra-cylindrical lens for the ABCD matrix was $f = 20$mm. The matrix for the lasing modes which pass through the extra-cavity cylindrical lens can be expressed as

$$M_x(z)=\begin{pmatrix}1 & z\\ 0 & 1\end{pmatrix}\cdot\begin{pmatrix}1 & d\\ 0 & 1\end{pmatrix} \tag{8}$$

and

#197102 - $15.00 USD Received 13 Sep 2013; revised 25 Oct 2013; accepted 5 Nov 2013; published 12 Nov 2013

$$M_y(z) = \begin{pmatrix} 1 & z \\ 0 & 1 \end{pmatrix} \cdot \begin{pmatrix} 1 & 0 \\ -1/f & 1 \end{pmatrix} \cdot \begin{pmatrix} 1 & d \\ 0 & 1 \end{pmatrix} \tag{9}$$

, where d is the distance of 2 cm from the beam waist to the extra-cavity cylindrical lens. The transverse profile of the astigmatic $HG_{0,0}$ mode can be converted to a circular-symmetric distribution at the far field by using of a single extra-cavity cylindrical lens. We employed the same concept to address the astigmatic high-order HG mode. Figures 5(a)–5(e) show the experimental transverse profile of the astigmatic $HG_{0,6}$ mode from the near field to the far field after transformation. The cavity length and the pump offset were fixed at $8\,\mathrm{mm}$ and $105\,\mu\mathrm{m}$, respectively. The transverse profile of the astigmatic $HG_{0,6}$ mode gradually became an elliptically shaped distribution at the position $z = 12\,\mathrm{cm}$, and the elliptically shaped distribution subsequently became a doughnut-shaped distribution, which is the LG mode.

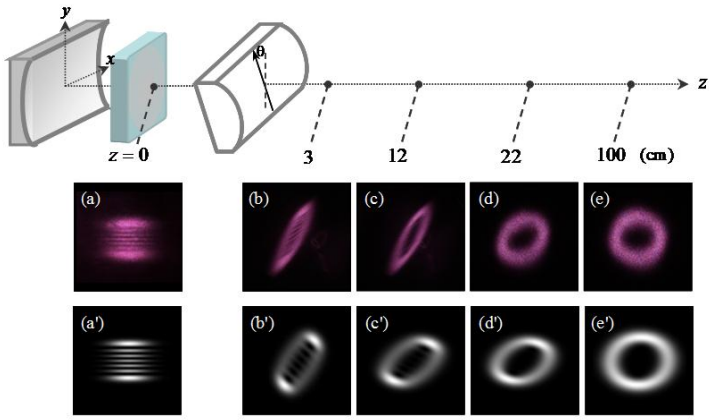

Fig. 5. (a)–(e): Experimental results for the transformation from the astigmatic $HG_{0,6}$ mode to the LG mode. (a')–(e'): Numerically reconstructed patterns for the experimental results.

Figures 5(a')–5(e') show the numerical results. The corresponding parameters of the numerical results were set as $R_x = 500\ \mathrm{mm}$, $R_y = 12\ \mathrm{mm}$, and $\theta = 40^{\circ}$. The transverse profile remained the same after position $z = 100\,\mathrm{cm}$. The theoretical analysis clearly demonstrated the effect of the single extra-cavity cylindrical lens, which was designed to transform the astigmatic high-order HG modes into high-order LG modes. Although we developed a novel experimental approach for converting astigmatic HG modes to LG modes, the output beam was not perfect. In Fig. 6 we show the phase structures for the transformed beam shown in Fig. 5(e') and for a pure LG mode to clarify the difference. The phase singularity of a pure LG mode was located at the center; the phase singularity of the transformed LG mode was not located at the center, but it splits into six phase singularities near the center.

A larger pump offset was used to achieve the high-order modes. Figures 7(a)–7(d) show the experimental transverse profile of the extremely high-order astigmatic HG mode from the

#197102 - $15.00 USD Received 13 Sep 2013; revised 25 Oct 2013; accepted 5 Nov 2013; published 12 Nov 2013

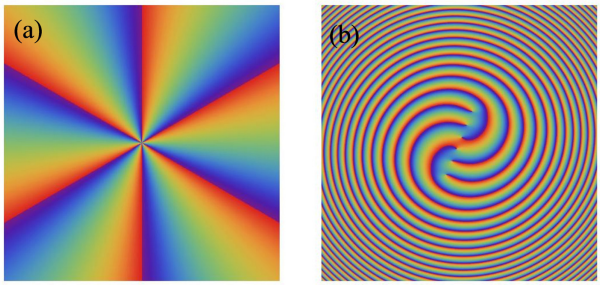

Fig. 6. (a): Phase distribution of a pure LG mode with an azimuthal index of 6. (b): Phase distribution of the numerical result for the transformed LG mode shown in Fig. 5(e').

near field to the far field after transformation. The propagation positions were $z = 0$, $1\,\mathrm{cm}$, $10\,\mathrm{cm}$, and $100\,\mathrm{cm}$, corresponding to the Figs. 7(a) to Figs. 7(d). The cavity length and the pump offset were fixed at $8\,\mathrm{mm}$ and $300\,\mu\mathrm{m}$, respectively. The index of the astigmatic HG mode was determined to be $HG_{0,47}$ by counting the nodes of the transverse pattern. Figures 7(a')–7(d') show the numerical results. The corresponding parameters of the numerical results were set to $R_x = 1000\ \mathrm{mm}$, $R_y = 12\ \mathrm{mm}$, and $\theta = 40^{\circ}$. The experimental patterns and the numerical results were similar in appearance, but slightly differed in structure. According to the overlapping feature shown in Fig. 7(a) and the spot-like pattern shown in Fig. 7(d), the experimental result is reasonably assumed to be the transformation from the superposed HG modes to the superposed LG modes. The method of using a pair of cylindrical lenses as a mode converter to transform HG and LG modes has been developed and applied in optical systems [32–34]. The theoretical analyses of a general astigmatic system have been discussed in several studies [28, 35,36]. However, this is the first study to generate astigmatic HG beams from a hemi-cylindrical cavity and transform the input beam to high-order LG beams using a single extra-cavity cylindrical lens. When using this method, the azimuthal index of the LG mode was over 40.

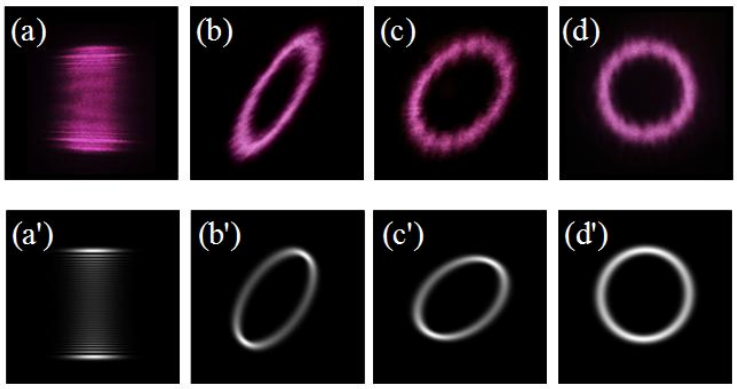

Fig. 7. (a)–(d): Experimental results for the transformation from the astigmatic $HG_{0,47}$ mode to the LG mode. The positions were $z = 0$, $1\ \mathrm{cm}$, $10\ \mathrm{cm}$, and $100\ \mathrm{cm}$. (a')–(d'): Numerically reconstructed patterns for the experimental results.

Previous research has revealed that the superposition of eigenmodes is ubiquitous in degenerate cavities [37–39]. We extended this observation into the concept of superposition of LG modes. In addition to doughnut-like LG modes, another type of complex optical mode can be generated using the method involving a defocusing pump. Figure 8(a) shows the

#197102 - $15.00 USD Received 13 Sep 2013; revised 25 Oct 2013; accepted 5 Nov 2013; published 12 Nov 2013

unique transverse profile at the far field. The numerical result shown in Fig. 8(b) indicates the superposition of two astigmatic HG modes, $HG_{1,2}$ mode and $HG_{0,11}$ mode, used

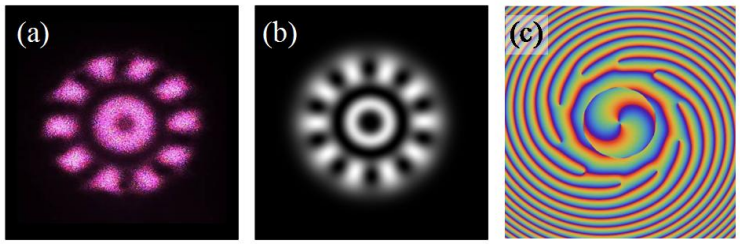

Fig. 8. (a): Experimental result for the transformation from the superposed astigmatic HG modes, $HG_{1,2}$ mode and $HG_{0,11}$ mode. (b): Numerically reconstructed pattern of (a). (c): Phase distribution of (b).

to reconstruct the experimental result. The numerical result qualitatively agrees with the experimental result. Figure 8(c) depicts the phase distribution of the numerical result. The phase singularities were arranged at the center and the dark points of the outer ring of the transverse profile. The superposition of the high-order LG modes was demonstrated by using the astigmatic cavity and a single cylindrical lens.

In addition, Figs. 9(a)–9(d) show several unique flower-type modes, which resulted from using a high degree of defocusing pump at the far field. Therefore, regarding the superposition of the LG modes, the off-axis and defocusing pumps are the primary reasons for the generation of these flower-type modes. The offset for generating these modes was set to approximately $250\,\mu\mathrm{m}$. The symmetry of these flower-type modes resulted from the longitudinal-transverse coupling of degenerate cavities. The longitudinal-transverse coupling usually leads to the frequency locking among different transverse modes with the help of different longitudinal orders [37]. The degeneracies for Figs. 9(a)–9(d) were fixed at

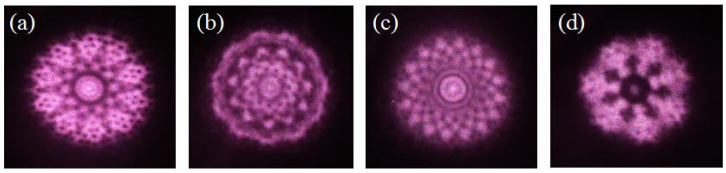

Fig. 9. (a)–(d): Experimental transverse patterns of the flower-type modes at the far field. The cavity lengths are (a): 7.9 mm, (b): 6.9 mm, (c): 8.5 mm, (d): 7.5 mm.

$\Delta\nu_T/\Delta\nu_L = 3/10$, $3/11$, $5/16$, and $2/7$, respectively. The $\Delta\nu_T$ is the transverse mode spacing, and the $\Delta\nu_L$ is the longitudinal mode spacing. In a hemi-cylindrical cavity the $\Delta\nu_T/\Delta\nu_L$ can be expressed as $(1/\pi)\cos^{-1}\left(\sqrt{1-L/R_y}\right)$. Figure 10 shows the far field patterns for the superposition of the anisotropic HG modes without the extra-cavity cylindrical lens in degenerate cavities corresponding to Fig. 9. It revealed that the far-field patterns for the superposition of the anisotropic HG modes emitted from degenerate cavities are difficult to indicate any difference from each other. However, the distribution of the far-field pattern shown in Fig. 10 indicated some concepts for numerical reconstruction. The components of the superposed modes are extremely high-order in the y direction because the pump offset for generating these modes are only in the y-axis direction. Using the extra-cavity cylindrical lens leads to the formation of the flower-type patterns which are transformed from the superposition of the anisotropic HG modes in degenerate cavities. We use the concept of

#197102 - $15.00 USD Received 13 Sep 2013; revised 25 Oct 2013; accepted 5 Nov 2013; published 12 Nov 2013

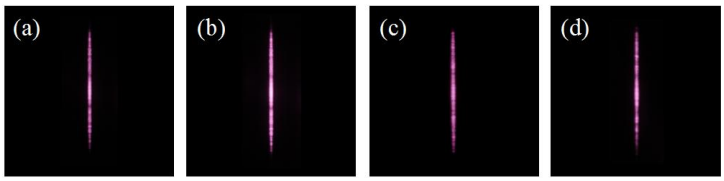

Fig. 10. (a)–(d): The far-field patterns for the superposition of the anisotropic HG modes in degenerate cavities without the added cylindrical lens corresponding to Figs. 9(a) –9(d).

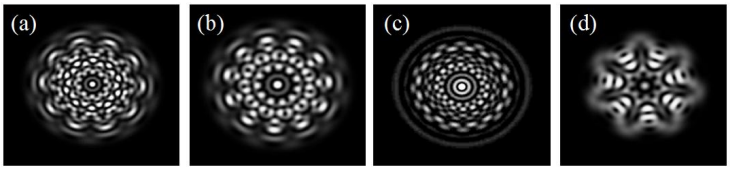

Fig. 11. Numerical results for the patterns transformed from the superposed astigmatic HG modes at far field. (a): $HG_{5,5} + HG_{5,15} + HG_{5,25} + HG_{5,35}$, (b): $HG_{3,3} + HG_{3,14} + HG_{3,25} + HG_{3,36}$, (c): $HG_{6,6} + HG_{6,22}$, (d): $HG_{2,2} + HG_{2,9} + HG_{2,16} + HG_{2,23} + HG_{2,30}$.

longitudinal-transverse coupling to superpose the degenerate anisotropic HG modes. Figure 11 show the numerical results according to the degenerate cavities for the Figs. 9(a)–9(d). Figure 11 displays the 10-fold, the 11-fold, the 16-fold, and the 7-fold rotational symmetry, and the symmetries are the same for Figs. 9(a)-9(d). Because it is difficult to precisely determine the components of the complicated flower-type modes, the reconstructed results are not optimal so far. Analyses of the structure and components of these complicated transverse modes are interesting questions to be considered in future studies.

5. Conclusion

In conclusion, we used a hemi-cylindrical laser cavity with an extra-cavity cylindrical lens to transform astigmatic HG beams into LG beams. By performing experimental-theoretical analysis, the transverse laser patterns were systematically reconstructed. In addition, we manipulated the order and the complexity of the lasing modes converted using a simple optical system by controlling the pump offset and the degree of defocus. The experimental results revealed that the unique flower-type laser patterns generally originate from a superposition of high-order LG modes which are transformed from the superposition of anisotropic HG modes in degenerate cavities. The proposed method is expected to be constructive for generating structured light that carries orbital angular momentum and optical vortices in several applications. By using the analogy between optical waves of laser cavities and quantum waves in a mesoscopic system, this study provides informative insights into investigating the wave nature of quantum systems.

Acknowledgments

This work is supported by the National Science Council of Taiwan (grant no: NSC-101-2112-M-003-001-MY3).

#197102 - $15.00 USD Received 13 Sep 2013; revised 25 Oct 2013; accepted 5 Nov 2013; published 12 Nov 2013